Reaction mechanisms leading to 3-body exit channels in central collisions of ^{129}Xe $+^{nat}$ Sn at 12 MeV/u

J. D. Frankland, D. Gruyer(*), E. Bonnet and A. Chbihi for the INDRA Collaboration

Grand Accélérateur National d'Ions Lourds (GANIL), CEA/DRF-CNRS/IN2P3
Bvd. Henri Becquerel, 14076 Caen, France

Summary. — We attempt to ascertain whether well-known sub-Fermi energy reaction mechanisms (fusion-fission, quasifission, deep-inelastic reactions) can explain the cross-sections and other characteristics recently observed for 3-fragment exit channels of central ^{129}Xe $+ ^{nat}$Sn collisions from 8 to 25 MeV/u measured with INDRA. In a first step, we have simulated deep-inelastic and capture (fusion-fission and/or quasifission) reactions at 12 MeV/u using the Deep Inelastic Transfers model coupled with GEMINI++, which we compare with data using a detailed software simulation of the INDRA array. Although minimum-bias measured and simulated reaction cross-sections are in good agreement, the cross-sections for 3-fragment exit channels are largely underestimated by the simulation. Moreover, 90% of simulated 3-body events are associated with mid-peripheral deep-inelastic collisions, whereas the measured coincident light charged-particle yields are consistent with central collisions leading to fusion or quasifission. However the observed 3-body yield seems beyond the reach of standard statistical decay of the primary (quasi)fission fragments.

1. – Introduction

Recently [1] we studied events with three heavy fragments ($Z > 10$) containing most of the charge of the combined projectile and target nuclei, in central collisions of ^{129}Xe $+ ^{nat}$Sn between 8 and 25 MeV/u. The measured cross-section for such events is ~ 50 mb in this energy range, corresponding to $30 \sim 40\%$ of the selected sample of central collisions from 12 MeV/u and upwards [2]. Using a new Coulomb chronometry technique, it was shown that such 3-body events arise from sequential fission-like splitting of a heavy composite system and we were able to estimate the time-scale of the second splitting, as well as to reconstruct the charge distribution of the two intermediate nuclei

---

(*) Present address: INFN, Sezione di Firenze, via Sansone 1, I-50019 Sesto Fiorentino, Italy

1

produced in the initial step, which showed that the first splitting is highly asymmetric, surprisingly so for a quasi-symmetric entrance channel.

In this contribution we report on results of simulations performed in order to try to pin down the reaction mechanism(s) responsible for these observations. The entrance channel reaction was calculated using the Deep Inelastic Transfers model (hereinafter referred to as DIT) [3] which models deep-inelastic collisions in terms of stochastic nucleon transfers between projectile and target, leading to dissipation of kinetic energy and angular momentum, and fluctuations of the final mass, charge, velocity, excitation energy and spin of the resulting quasi-projectile and quasi-target. 10^5 collisions were calculated with a triangular distribution of entrance channel angular momenta $0 < \ell \leq \ell_{\max}$ with $\ell_{\max} = 519\hbar$ corresponding to a total reaction cross-section of 3831 mb. These values are very close to those given by the systematics of [4], as is the cross-section of 92 mb corresponding to central collisions for which projectile and target do not reseparate. In a first approach, we assume complete fusion to occur (^{129}Xe+^{nat}Sn $\rightarrow$ ^{248}Rf) as pre-equilibrium emission is not included in DIT (below we will present an alternative outcome for these events, see sect. **2**˙3). It may be noted that recent calculations predict a small but finite fission barrier B_f for element $Z = 104$ of between 4 and 6 MeV [5].

The statistical decay of the primary fragment(s) resulting from the entrance channel calculation was then calculated using GEMINI++ [6]. We used this statistical decay code out-of-the-box with no adjustment of any parameters and with all options taking their default values, as recommended by the authors. Each entrance channel calculation was "decayed" 5 times as a compromise between a good sampling of the possible decay chains and the length of computation. The resulting final events were then subjected to a random azimuthal rotation and boosted to the laboratory frame in order to simulate their detection by the INDRA multidetector [7], using the KaliVeda C++ toolkit [8]. This simulation is an accurate replication of the array geometry, identification thresholds and particle reconstruction procedures, including particle misidentification due to hits in the same or adjacent telescopes. Detectors or identification telescopes which did not function during the experimental runs were also excluded from the simulation. Experimental details can be found in [1].

2. – Comparison between simulations and data

The total measured reaction cross-section for collisions of ^{129}Xe $+$ ^{nat}Sn at 12 MeV/u with a minimum bias multiplicity trigger of $M \geq 2$ was calculated to be 1855 mb (using the measured integrated beam current in a Faraday cup, assuming the equilibrium charge state of the projectile after the target to be given by [9], correcting for acquisition dead time, and being careful to exclude beam pile-up —two or more projectile-like fragments detected in the same event— from the number of recorded triggers). For the simulations, the equivalent detected cross-section with the same trigger condition is 1754 mb (corresponding to 46% of the total simulated cross-section). As the two global cross-sections are very similar, in the following we will present all comparisons between experiment and theory in terms of absolute cross-section, without any normalisation.

2˙1. *Events with 2-body kinematics*. – In fig. 1 (top row) we study the correlations between azimuthal angle and atomic number for the two heaviest detected fragments of each event. By considering the relative azimuthal angle $|\phi_1 - \phi_2|$ we can identify events where the kinematics of the two heaviest fragments are dominantly 2-body in nature: in this case $|\phi_1 - \phi_2| \sim 180°$ signals that the fragment momenta lie on opposite sides of
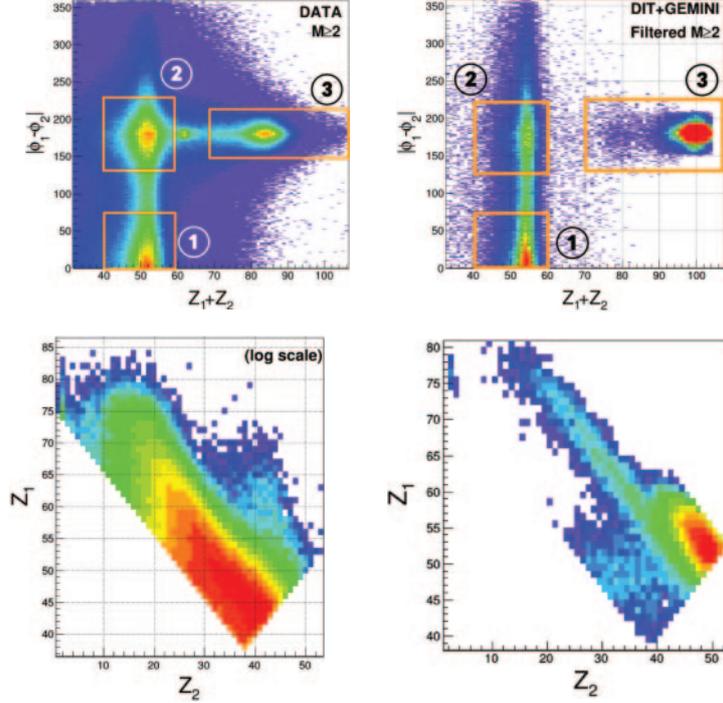
Fig. 1. – Top row: Correlations between the azimuthal angles and atomic numbers of the two heaviest fragments detected in each minimum bias triggered event, for experimental (left) and simulated (right) data. Bottom row: Correlation between the atomic numbers of the two fragments in Zone 3 for experimental (left) and simulated (right) data.

the beam direction in a common (reaction) plane. Correlating this quantity with the total charge of the two fragments, $Z_1 + Z_2$, allows to determine whether such events are truly 2-body in nature ($Z_1 + Z_2 \sim Z_{proj} + Z_{targ}$) or only concern a subset of the true event, which was not fully detected ($Z_1 + Z_2 \sim Z_{proj}$: due to detection/identification thresholds, the heaviest fragments in incompletely measured events result mainly from the decay of projectile-like fragments).

We can note in fig. 1 (top row) that fluctuations in experimental data are far greater than for the simulation. Nevertheless clear similarities exist between the two, notably in the accumulation of events in three zones which we have labelled in the figure. Zones 1 and 2 concern incompletely detected events with $Z_1 + Z_2 \sim Z_{proj}$. In the simulation these zones are populated mostly by a projectile-like fragment (PLF) residue or fission fragment detected in coincidence with either a light charged particle (LCP) or intermediate mass fragment (IMF: $3 \leq Z \leq 20$). There is also a contribution from fusion-fission reactions, which manifests almost exclusively as detection of one of the fission fragments of the ^{248}Rf compound nucleus ($45 \leq Z \leq 55$) in coincidence with an evaporated α-particle. The experimental Z_1-Z_2 correlations are similar to those of the simulation, but with a far more important production of coincident IMF. It should be noted also that a strong contribution of fragments with $40 \leq Z \leq 60$ detected in coincidence with an α-particle is also seen in the experimental data, although attributing this to a precise reaction mechanism is of course hazardous.
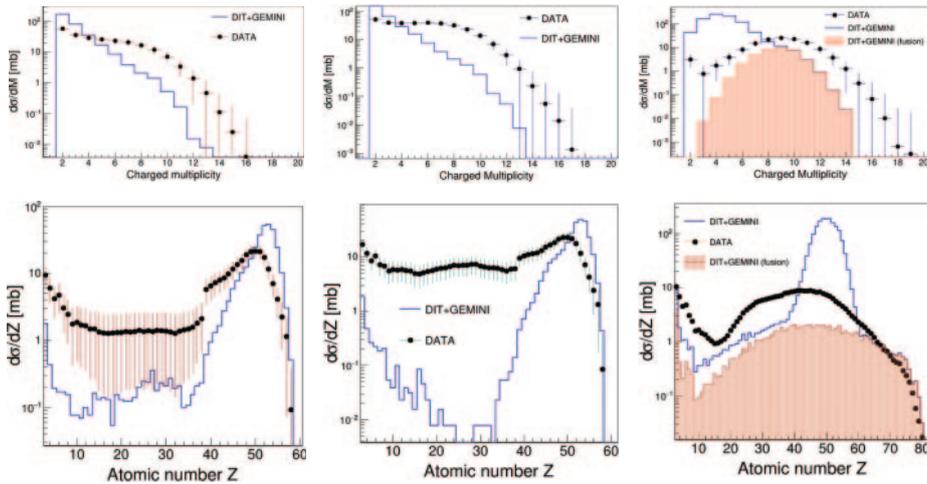
Fig. 2. – Comparison of experimental and simulated charged product multiplicity (top row) and yield (bottom row) distributions for events in the 3 zones of fig. 1: zone 1 (left), zone 2 (middle), zone 3 (right).

Zone 3 is the most interesting as for these events the two heaviest detected fragments contain the majority of the entrance channel nucleons, thus allowing a full reconstruction of the event. The population of this zone is quite different for data and simulation: whereas simulated events are strongly concentrated around $Z_1 + Z_2 \sim 100$, the experimental data show an accumulation at $Z_1 + Z_2 \sim 84$. The correlations between Z_1 and Z_2 for zone 3 are shown in fig. 1 (bottom row). In the simulated events (right column), these correlations can be separated into three diagonal zones corresponding to different values of $Z_1 + Z_2$. Events with $Z_1 + Z_2 > 100$ are deep-inelastic collisions for which both PLF and TLF (target-like fragment) are detected and identified; events with $Z_1 + Z_2 < 90$ are also deep-inelastic collisions, but where one of PLF or TLF has undergone fission (3-fragment event). Sandwiched in between these two zones is a very broad region with $Z_1 + Z_2 \sim 94$: these events correspond to fusion-fission. Comparing with the experimental data (left column) we remark that the zone of large $Z_1 + Z_2 > 95$, although present, is far less populated. The majority of events populate a broad distribution of (Z_1, Z_2) values with $Z_1 + Z_2 < 95$, with perhaps an indication of the presence of a second, less broad distribution for $Z_1 + Z_2 < 82$.

Figure 2 compares the charged-particle multiplicity distributions and charged-product yield distributions zone by zone. The multiplicity can be taken as a rough measure of the amount of energy dissipated into excitation energy by the reactions; on this basis we can say that for zones 1 and 2, dominated by deep-inelastic collisions, the DIT model is not sufficiently dissipative. In zone 3 we highlight the part of the simulated distribution which is due to fusion alone: although not as broad as the experimental distribution, we can remark that the centroids of the two distributions are very close. On the other hand, the low-multiplicity bump in the simulation, which corresponds to well-detected deep-inelastic collisions with $Z_1 + Z_2 \sim 100$ discussed above (see fig. 1), is completely absent from the experimental data.

The charged product yields (fig. 2, bottom row) also show large differences between data and simulation. For zones 1 and 2 the experimental PLF bump for $Z > 40$ has
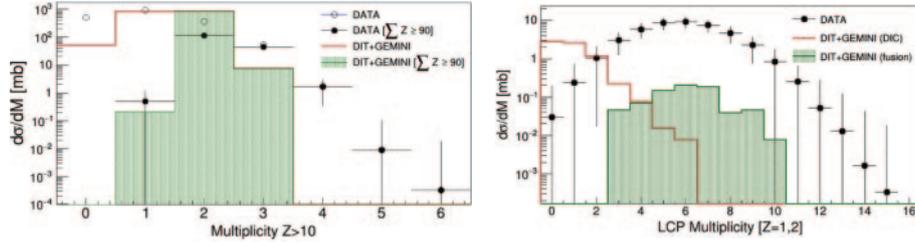
Fig. 3. – (left) Multiplicity distributions for heavy fragments with $Z > 10$; (right) Multiplicity of coincident light charged particles in well-detected events ($\sum_i Z_i \geq 90$) with 3 heavy fragments ($Z > 10$) in the exit channel.

a maximum which is shifted to lower Z values and a broader distribution than in the simulation, although a good agreement on the upper Z limit of these fragments can be noted. However the main disagreement occurs for the yields in the range $10 \leq Z \leq 40$ where data show a significant contribution centred at $Z \sim 25$–30: a small yield of such fragments is present in zone 1 in the simulations, corresponding to fission fragments of the TLF detected in coincidence with a PLF residue, but they are completely absent from zone 2. It seems therefore that in the data there is far more TLF fission than in the simulations, which again indicates insufficient dissipation in the DIT model with possibly also an underestimation of the spin transferred to PLF and TLF. In the simulated yields for zone 3 we see again the high cross-section for detection of both PLF and TLF residues with atomic numbers not very different from projectile and target, which is entirely absent from data. This narrow bump for deep-inelastic collisions is accompanied by a very broad distribution of fission fragments coming from the fusion reactions. Although the experimental yield of all but the heaviest fragments is underestimated by the simulations, it should be noted that the yield of fragments with $Z \geq 65$ is remarkably well-reproduced.

2·2. *Events with 3 heavy fragments.* – Figure 3 (left) shows the multiplicity distributions for heavy fragments defined as $Z > 10$. These are shown with and without the requirement to have detected nearly all charged products of each event, $\sum_i Z_i \geq 90$. The model overestimates the cross-section for 2-fragment events (847 mb instead of 113 mb) and underestimates that for 3 fragments (8 mb instead of 43 mb) (all cross-sections are for well-measured events with $\sum_i Z_i \geq 90$). Moreover, in the data up to 6 coincident heavy fragments are observed: no more than 3 are seen in the simulation. Concerning the origin of the 3-fragment events, in the simulation 90% of them result from PLF or TLF fission following a mid-peripheral deep-inelastic collision, for which the primary fragment spins reach a maximum. Only 10% (0.8 mb) are the result of sequential fission of the compound nucleus formed in fusion events. The two cases can be clearly distinguished by the coincident light charged particle multiplicity, which roughly measures the excitation energy generated in the reaction (fig. 3 (right)). Fusion events have a much higher associated mean LCP multiplicity. The experimental multiplicity distribution for 3-fragment events, although much broader, has a very similar shape and mean value to the simulated fusion-sequential fission events. Fragment charge distributions (see fig. 4 (left)), on the other hand, are not well-reproduced by either reaction mechanism, with a notable lack of yield for heavy fragments with $Z > 60$.
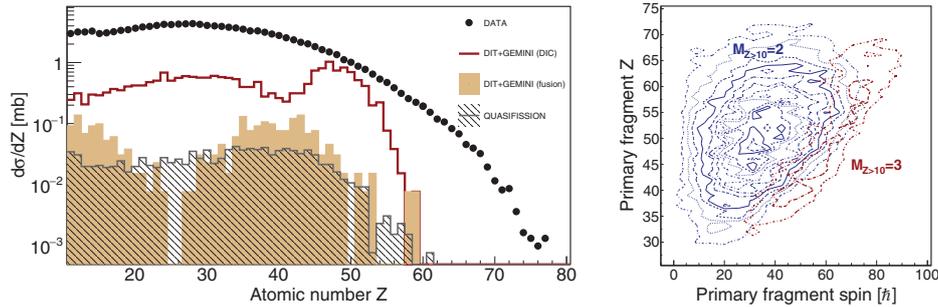
Fig. 4. – Left: Experimental and simulated heavy fragment yield distributions for well-measured ($\sum_i Z_i \geq 90$) events with 3 heavy fragments ($Z > 10$) in the exit channel. Right: Primary fragment atomic number and spin correlations for simulated quasifission events leading to 2 or 3 heavy fragments.

2˙3. *Quasifission simulations.* – In the previous paragraphs we have seen that neither deep-inelastic collisions nor fusion-fission reactions can account for both the cross-section and associated dissipation/excitation energy which are experimentally observed for the 3-fragment events studied in [1]. As noted above, DIT tells us nothing about the outcome of reactions which do not lead to a deep-inelastic collision, and up to now we have assumed that these "capture" reactions lead to complete fusion. The other extreme is to assume that they all result in quasifission, which we have simulated with a phenomenological ansatz based on the literature [10,11].

In this toy model, the fragment mass distribution broadens with decreasing entrance channel angular momentum from the deep-inelastic width given by DIT at $\ell = \ell_{\rm cr}$ (the angular momentum for which the attractive pocket in the adiabatic nucleus-nucleus potential [12] disappears) up to the width for compound nucleus fission given by GEMINI++ at $\ell = 0$. The angular momentum converted to fragment spin is calculated with the sticking limit [13] (using spherical moments of inertia). The total centre-of-mass kinetic energy of the fragments after separation is taken from fission systematics [14]. Then the available thermal excitation energy is deduced by energy conservation taking into account the mass balance, and shared in the ratio of the fragments' mass. Finally, the direction of the centre-of-mass separation axis was drawn at random in the reaction plane (fission-like distribution).

After statistical decay by GEMINI++ and simulated detection by INDRA, these quasifission events produce a 3-fragment cross-section (for well-measured events with $\sum_i Z_i \geq 90$) of only 0.4 mb, half of that produced by fusion-fission, and only 1% of the experimental value. The associated LCP multiplicity distribution is very similar to that for fusion, whereas the fragment charge distribution (fig. 4 (left)) is flatter and more resembles the form of the experimental one, although there is still no yield for fragments with $Z > 60$. One way to increase the cross-section for 3-fragment events is by (artificially) increasing the spin transfer to the primary fragments: if we suppose that all entrance channel angular momentum is converted to intrinsic spin, the cross-section increases by a factor of 10 (4 mb instead of 0.4 mb, compared to the experimental 43 mb). In this case (fig. 4 (right)) it can be seen that selecting 3-fragment events favours primary fragments with the largest spin; in addition, the corresponding primary fragment Z-distribution is asymmetric, although the initial distribution created by our quasifission simulation is symmetric.

3. – Conclusions

In our simulations we have identified three possible reaction mechanisms to explain the observed events with 3 heavy ($Z > 10$) fragments in ^{129}Xe$+^{nat}$Sn collisions at $12\,\mathrm{MeV/u}$: mid-peripheral deep-inelastic collisions followed by fission, complete fusion followed by sequential fission, and quasifission followed by fission. Mid-peripheral collisions can be excluded because of the measured coincident light charged particle multiplicities, which are only well-reproduced by capture reactions leading to fusion or quasifission. However, the associated cross-sections are still greatly underestimated by the simulations. The limiting factor seems to be the probability of the second/last splitting, which in both cases is calculated by the statistical decay model assuming an initially equilibrated hot nucleus. In the framework of the statistical model, fission is favoured over other decay channels for heavy nuclei with large angular momentum. We have seen that increasing the spin transfer beyond physically meaningful limits in the quasifission toy model has a large effect on the 3-fragment cross-section, as well as "asymmetrizing" the initially symmetric quasifission fragment mass distribution. Even so, reproducing the experimental yield in this way would require total capture cross-sections of ≥ 1 barn, far greater than are expected from systematics for this system. It seems therefore more likely that some dynamical effect, not taken into account in these simulations, is responsible for producing highly-deformed primary fragments in the first step so that the probability of a second fission-like splitting is greatly enhanced. More sophisticated calculations [15] should be carried out in order to test this hypothesis.

$$* * *$$

REFERENCES

[1] GRUYER D. et al., Phys. Rev. C, **92** (2015) 064606.
[2] CHBIHI A. et al., JPCS, **420** (2013) 012099.
[3] TASSAN-GOT L. et al., Nucl. Phys. A, **524** (1991) 121.
[4] WILCKE W. W. et al., At. Data Nucl. Data Tables, **25** (1980) 389.
[5] ITKIS M. G. et al., Phys. Rev. C, **65** (2002) 044602; KOWAL M. et al., Phys. Rev. C, **82** (2010) 014303.
[6] CHARITY R. J., Phys. Rev. C, **82** (2010) 014610; MANCUSI D. et al., Phys. Rev. C, **82** (2010) 044610.
[7] POUTHAS J. et al., Nucl. Instrum. Methods Phys. Res. A, **357** (1995) 418.
[8] KaliVeda data analysis toolkit, `http://indra.in2p3.fr/KaliVedaDoc`.
[9] LEON A. et al., At. Data Nucl. Data Tables, **69** (1998) 217.
[10] GREGOIRE C. et al., Nucl. Phys. A, **387** (1982) 37.
[11] TÕKE J. et al., Nucl. Phys. A, **440** (1985) 327.
[12] BONDORF J. P. et al., Phys. Rep., **15** (1974) 83; BŁOCKI J. et al., Ann. Phys. (N.Y.), **105** (1977) 427.
[13] MORETTO L. G. et al., Rep. Prog. Phys., **44** (1981) 533.
[14] VIOLA V. E. et al., Phys. Rev. C, **31** (1985) 1550; HINDE D. J. et al., Nucl. Phys. A, **472** (1987) 318.
[15] MAZUREK K. et al., Phys. Rev. C, **84** (2011) 014610; NADTOCHY P. N. et al., Phys. Rev. C, **85** (2012) 064619.